A Theoretical Study of the Monohydration of Mercury Compounds of Atmospheric Interest

Sonia Taamalli, [†,*] *Michal Pitoňák,* [¶,‡] *Theodore S. Dibble,* [§] *Ivan Černušák,* [¶] *Florent Louis* [†]

[†]Univ. Lille, CNRS, UMR 8522 - PC2A - PhysicoChimie des Processus de Combustion et de l'Atmosphère, 59000 Lille, France

[§]Department of Chemistry, State University of New York-College of Environmental Science and Forestry, 1 Forestry Drive, Syracuse, New York 13210, United States

[¶] Department of Physical and Theoretical Chemistry, Faculty of Natural Sciences, Comenius University in Bratislava, Ilkovičova 6, 84215 Bratislava, Slovakia

[‡]Computing Center, Centre of Operations of the Slovak Academy of Sciences, Dúbravská cesta 9, 845 35 Bratislava, Slovakia

Abstract

The structures, vibrational frequencies and model IR spectra of the monohydrates of oxygenated mercury compounds (BrHgO, BrHgOH, BrHgOOH, $BrHgNO_2$, BrHgONO, and HgOH) have been theoretically studied using the ωB97X-D/aug-cc-pVTZ level of theory. The ground state potential energy surface exhibits several stable structures of these monohydrates. The thermodynamic properties of the hydration reactions have been calculated at different levels of theory including DFT and coupled-cluster calculations DK-CCSD(T) with the ANO-RCC-Large basis sets. Standard enthalpies and Gibbs free energies of hydration were computed. The temperature dependence of $\Delta_r G°(T)$ was evaluated for the most stable complexes over the temperature range 200 - 400 K. Thermodynamic data revealed that the highest fraction hydrated at 298 K and 100% relative humidity will be $BrHgNO_2$-H_2O at ~5%. Atmospheric implications have been discussed.

I. INTRODUCTION

Mercury is a neurotoxin that bioaccumulates in fish to levels that can be hazardous to wildlife and humans that consume fish.[1,2] The atmosphere can transport mercury, mostly in the form of elemental Hg(0), far from the location of emissions to sites where mercury concentrations are low. As a result, the atmospheric transport of mercury strongly influences its global biogeochemical cycling. The lifetime of mercury in the atmosphere is largely controlled by its redox chemistry, due to the much higher deposition efficiency of Hg(II) (+2 oxidation state) compounds as compared to Hg(0).[3,4] There have been many recent studies of gas-phase complexes of water with atmospherically relevant trace gases and radicals, although in relatively few cases do these complexes occur to such an extent and with such effect as to influence atmospheric chemistry.[5] Major exceptions to this generalization include water dimer,[6] catalysis of the HOO self-reaction,[7,8] reactions of Criegee intermediates,[9] and nucleation of new

particles.[10,11] One motivation of the present studies of complexes of water with mercury compounds is to determine whether these complexes could influence the gas-phase chemistry of mercury.

Scientists currently believe that Hg(0) oxidation is mainly initiated by atomic bromine, to yield stable Hg (II) compounds such as BrHgOH, BrHgOOH, and BrHgONO.[3,4,12–14] BrHgONO has two conformers (syn and anti) and an isomer ($BrHgNO_2$).[15] Photolysis of BrHgONO[16,17] and BrHgOOH[17] can produce the radical BrHgO. Initiation of Hg(0) oxidation by hydroxyl radical leads to a Hg(I) radical intermediate: HgOH.[14] Goal of this paper is to investigate the monohydration of these seven mercury compounds.

The last several years have seen major advances in our understanding of the gas-phase mechanisms of mercury chemistry in the atmosphere,[3,14,17–19] but less so for its heterogeneous and aqueous-phase chemistry. Key exceptions involve mechanistic studies of dry surfaces of minerals,[18] but these investigations were carried out on dry surfaces. This does limit the immediate environmental importance of these studies, because surface water[19,20] will probably exert a strong influence on surface reactivity and binding of Hg (II) compounds. This provides another motivation for our work: computational studies of the surface chemistry and physics of mercury require highly efficient methods whose accuracy cannot be assured *a priori*. The accurate binding energies determined in the present work can be used to validate computational approaches for the study of the surface chemistry of mercury.

Only two of the mercury species to be studied here have ever been detected in the laboratory[21,22] (in aqueous solution) and there have been no previous experimental or computational studies of their microsolvation. Previous studies of hydration of mercury and its compounds have mostly focused on solvation in the bulk aqueous phase,[23–27] although most of these studies also consider gas-phase complexes with a single water molecule. However, none of these

investigations considered the mercury compounds being studied here. As a first step towards understanding these interactions, we theoretically study the monohydration process of several oxygenated mercury-containing compounds as follows:

$$BrHgO + H_2O \rightarrow BrHgO\_1w \quad (R1)$$

$$BrHgOH + H_2O \rightarrow BrHgOH\_1w \quad (R2)$$

$$BrHgOOH + H_2O \rightarrow BrHgOOH\_1w \quad (R3)$$

$$Anti\text{-}BrHgONO + H_2O \rightarrow Anti\text{-}BrHgONO\_1w \quad (R4)$$

$$Syn\text{-}BrHgONO + H_2O \rightarrow Syn\text{-}BrHgONO\_1w \quad (R5)$$

$$BrHgNO_2 + H_2O \rightarrow BrHgNO_2\_1w \quad (R6)$$

$$HgOH + H_2O \rightarrow HgOH\_1w \quad (R7)$$

We use the suffix 1w to refer to the monohydrated molecule, as we plan to investigate the addition of more waters to some of these molecules. Immediately below, we present the details of the methods used in this work. Next, we describe the structures and thermodynamic properties of the monohydrates. Finally, we discuss the implications of this hydration process to mercury chemistry in the atmosphere.

II. COMPUTATIONAL DETAILS

Geometry optimizations were carried out for seven species (BrHgO, BrHgOH, BrHgOOH $BrHgNO_2$ and its isomers, and HgOH) and their complexes with one water molecule. For each species and its complexes, structures and harmonic vibrational frequencies were computed using the density functional theory (DFT) with the long-range corrected (LC) hybrid functional ωB97X, with the addition of an empirical dispersion correction (ωB97X-D)[28] in Gaussian16.[29] This hybrid functional is suitable for non-covalent interactions.[30,31] Dunning's aug-cc-pVTZ basis sets were used for H and O atoms.[32,33] To account for scalar relativistic effects in Hg and

Br, we usedthe Stuttgart/Cologne scalar pseudopotentials for the 60 innermost electrons of Hg (ECP60MDF) and the 10 innermost electrons of Br (ECP10MDF); electrons outside the core were treated with the aug-cc-pVTZ-PP basis set.[32,34,35] The frozen-core approximation correlated only the 5d and 6s electrons of Hg, the 4s and 4p electrons of Br, and the valence electrons of H and O. As a starting point for the micro-hydration, we have calculated the electrostatic potential (ESP) maps for all seven species projected onto the electron density envelope at the contour value 0.02e. These maps carry useful initial information on the preferential solvation sites for water molecule, functioning either as proton donor or as electron donor. Based on this map, water molecule was placed around all the exterior atoms of these mercury compounds in different orientations. This generated many initial conformations for each structure.

For one of the mercury compounds, $BrHgNO_2$, this methodology was validated by quenched molecular dynamics protocol,[36] followed by unsupervised structural similarity analysis. By performing on-the-fly DFT molecular dynamics (MD) at temperatures ranging from 30 to 200 K using PBE functional[37–39] with D3 empirical dispersion correction[40] and DZVP basis set[41] in CP2K software package[42] the conformational space was extensively sampled. Random snapshots from MD were consequently optimized using D3-corrected B3LYP[40] and LanL2DZ basis set[43–46] in Gaussian16, and the resulting distance matrices used as a feature vectors in the follow-up *K-means* method of clustering analysis.[47,48] Clustering analysis was in accord with the potential surface minima found via the manual procedure described above, and no other stable geometries were discovered. In particular, placing the H_2O at bromine end of the oxygenated mercury molecules did not yield stable structure of any sought conformer.

Using the geometries obtained at the ωB97X-D/aug-cc-pVTZ level, energies were recalculated using Douglas-Kroll CCSD(T) with the all electron relativistic ANO-RCC-Large basis sets[49] available within MOLCAS software package.[50] We also applied the Goodson (continuous

fraction) formula[51] to the DK-CCSD(T)/ANO-RCC-Large results, enabling us to estimate the contribution to the full CI extrapolation (denoted CCSD(T)-cf in the rest of the article). Enthalpies and Gibbs free energies of hydration were computed using the rigid rotor-harmonic oscillator approximation. To reduce the error in thermodynamic quantities associated with the low-frequency modes we have used the quasi-rigid-rotor-harmonic-oscillator (QRRHO) treatment[52] as implemented in the Shermo code.[53] Within QRRHO, there is pre-defined cutoff for low-frequency modes and each mode below this cutoff is artificially raised to 100 cm^{-1}. This leads to more reasonable entropy contribution to free energies. Relative energies, enthalpies, and free energies presented below are at the DK-CCSD(T)-cf level of theory unless otherwise specified.

To elucidate the bonding within these complexes, we have performed localized molecular orbital energy decomposition analysis (LMOEDA) of the interaction energies[54] as implemented in GAMESS US code. These calculations were done at the MP2 level utilizing pseudopotential SBKJC-VDZ basis set[55]. Within LMOEDA the total interaction energy is decomposed to the following components: electrostatic E_C (dominated by the attractive Coulomb interaction between nuclei of each fragment and electrons of the other one), exchange E_X (due to anti-symmetry of the wave function allowing exchange of electrons), Pauli repulsion E_R, polarization E_P, dispersion E_D. We note that the attractive E_X component includes also the charge-transfer between the monomers.

III. RESULTS

III.1. Subsystems

ESP maps for all seven species are presented in Figure 1. The color coding reveals strong electron acceptor site on H and Hg, respectively, in accord with their low electronegativities. Oxygen and nitrogen atoms can serve as proton acceptors, while bromine with a weak positive

ESP value is expected to be unimportant to hydration by a single water molecule. There is a more or less visible σ-hole developed on Br atom for each species and its size depends on the number and position of N/O atoms on the opposite side of the molecule.

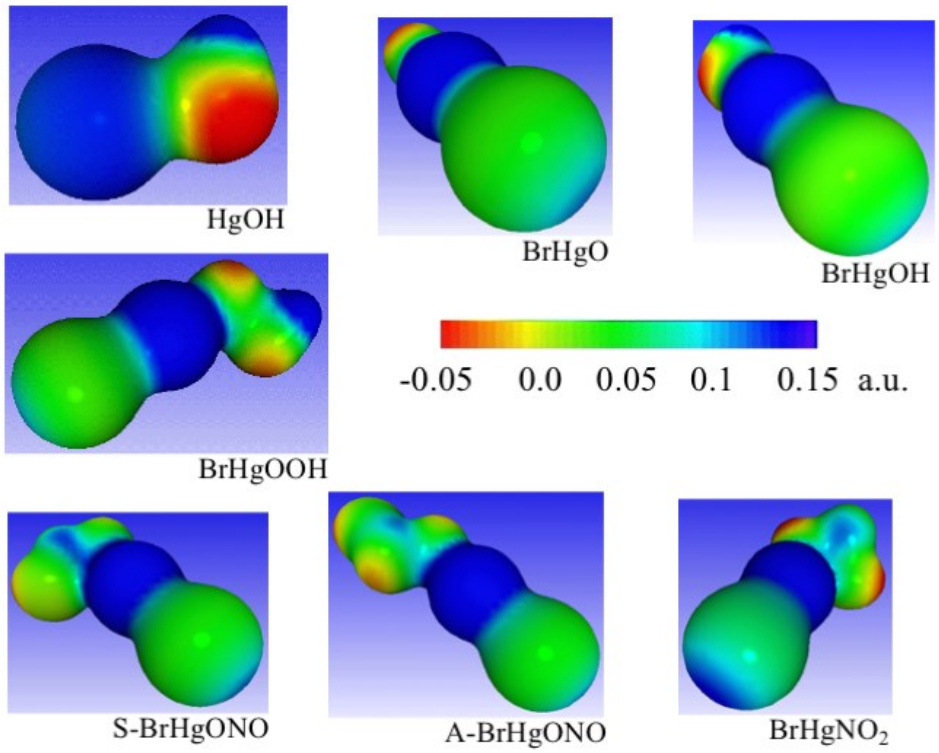

Figure 1. Color-coded electrostatic potential maps. The color scale ranges from the most negative (red) to the most positive (blue) potential.

In all Figures bond lengths are in Angstroms and bond angles are in degrees. All Figures of hydrated species also provide DK-CCSD(T)-cf/ANO-RCC-Large values of $\Delta_r H°$ (0 K) and of $\Delta_r G°$ (298 K) for the hydration in kJ mol^{-1}. The enthalpy values are always more negative than $\Delta_r G°$ in these Figures, due to the negative entropy of hydration. Optimized ωB97X-D/aug-cc-pVTZ geometries of all subsystem structures are collected in Figure 2 and their corresponding structural data (geometries and frequencies) are presented in Tables S1 and S2 of the Supporting Information. Model harmonic and/or anharmonic IR spectra for BrHgO, BrHgOH, BrHgOOH, HgOH, syn- and anti-BrHgONO and $BrHgNO_2$ are in Figures S1 and S2 of the Supporting

Information. Only harmonic spectrum is presented for BrHgO since the anharmonic treatment of linear tops is experimental in the current implementation.

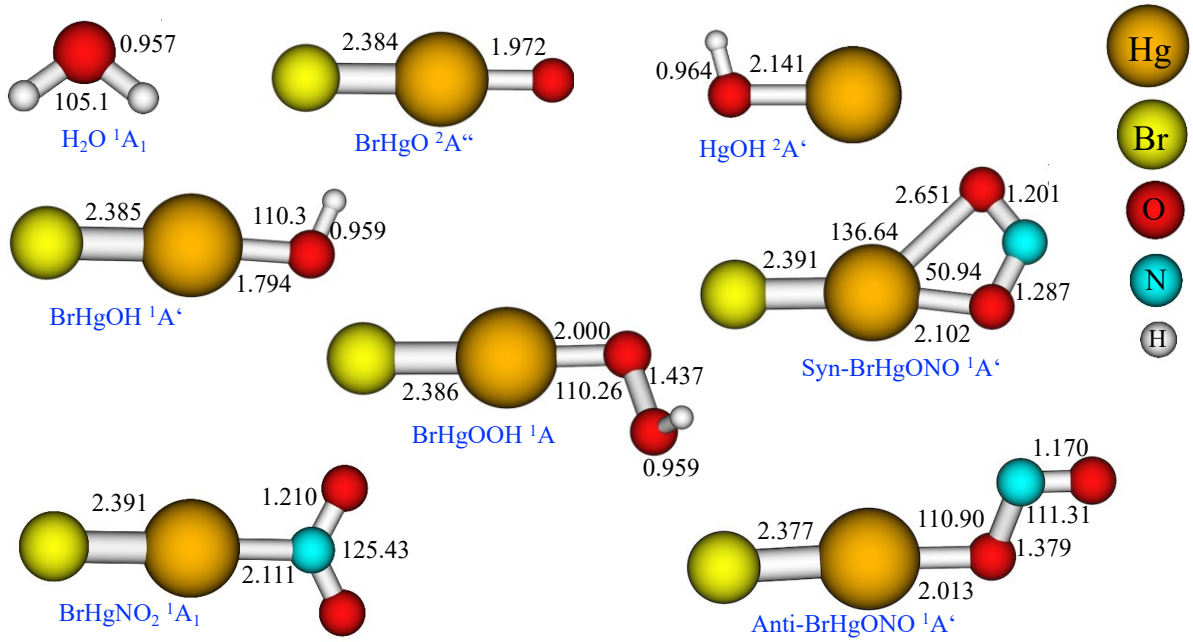

Figure 2. Structures of H_2O and mercury species optimized at the ωB97X-D/aug-cc-pVTZ level of theory. Color coding is in top right corner.

III.2. Complexes

The series of monohydrated BrHgO, BrHgOH and BrHgOOH species is shown in Figures 3-5 and will be discussed together because they exhibit gradual increase of hydration sites. Their model IR spectra are collected in Figures S3-S5 of the Supporting Information. In the case of complexes, the attempts to calculate the anharmonic IR spectra were not successful because of the symmetry breakdown during the numerical differentiation of the second derivatives when calculating the cubic and quartic force constants associated with the very shallow part of the potential energy surface. Therefore, we present only model harmonic IR spectra for all the complexes (Figures S3-S9). These model IR spectra in Figures S1-S9 can help experimental characterization of these compounds and their possible complexes with water.

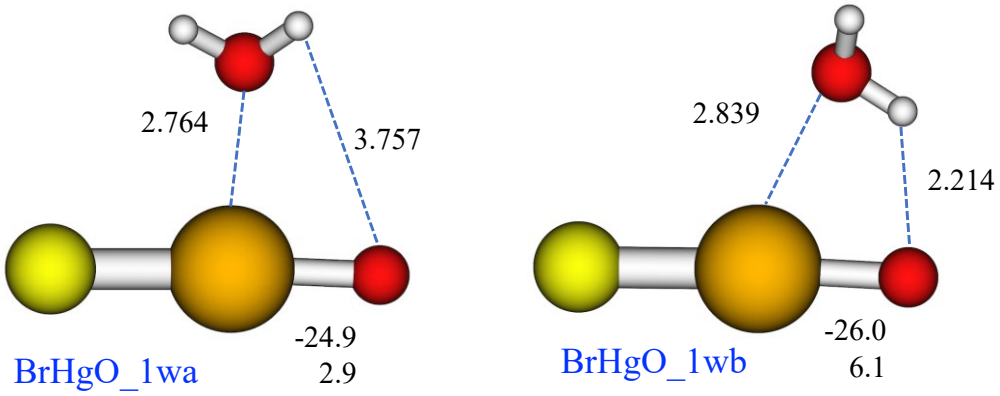

Figure 3. ωB97X-D/aug-cc-pVTZ optimized structures of BrHgO + H_2O molecular complexes. Atom color-coding as in Fig. 2.

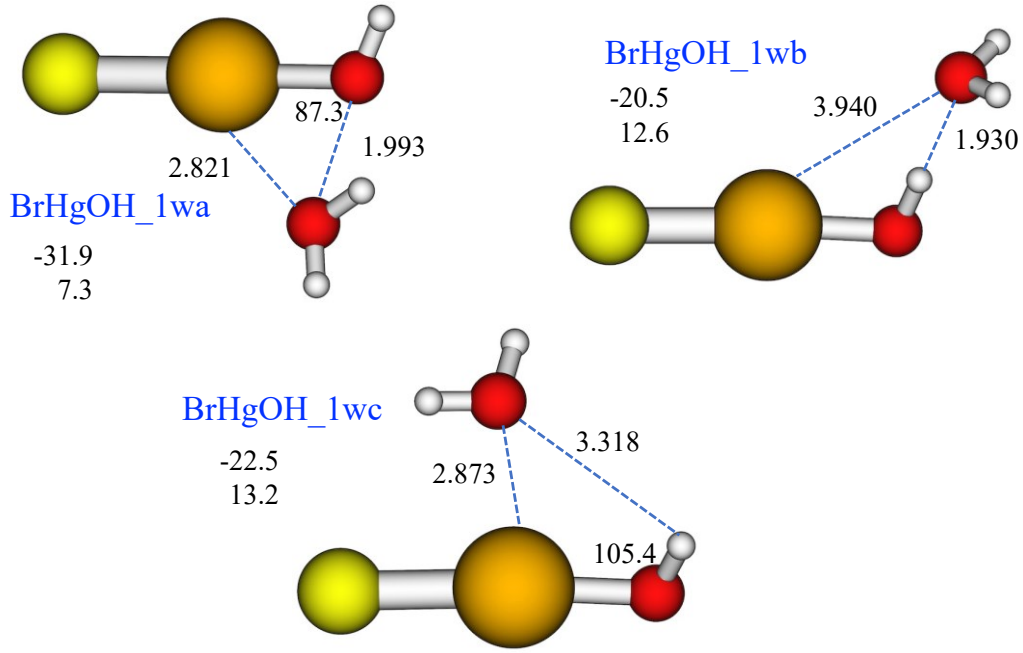

Figure 4. ωB97X-D/aug-cc-pVTZ optimized structures of BrHgOH + H_2O molecular complexes. Atom color-coding as in Fig. 2.

In Figures 6-8 we present the second series – monohydrated anti-BrHgONO, syn-BrHgONO and $BrHgNO_2$. In these complexes one can observe two modes of interaction: electron-donor (ED) from H_2O towards Hg and proton acceptor (PA) by ONO or NO_2 moiety. The most stable

complexes at the level of electronic energies (1wa) always prefer the combination of ED together with PA.

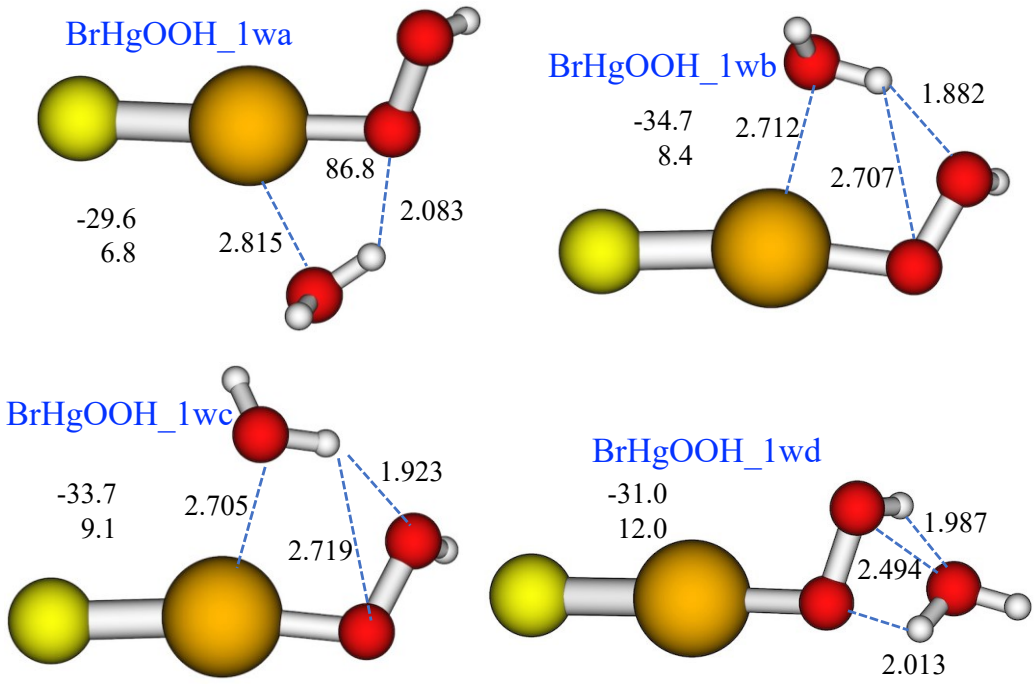

Figure 5. ωB97X-D/aug-cc-pVTZ optimized structures of BrHgOOH + H_2O molecular complexes. Atom color-coding as in Fig. 2.

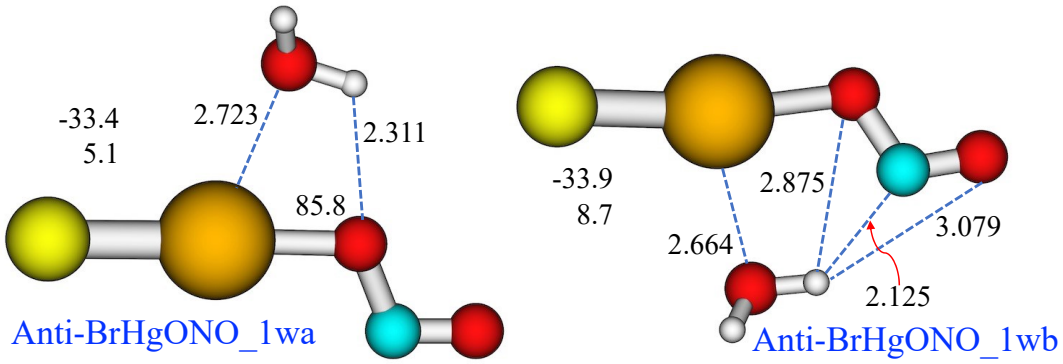

Figure 6. ωB97X-D/aug-cc-pVTZ optimized structures of anti-BrHgONO + H_2O molecular complexes. Atom color-coding as in Fig. 2.

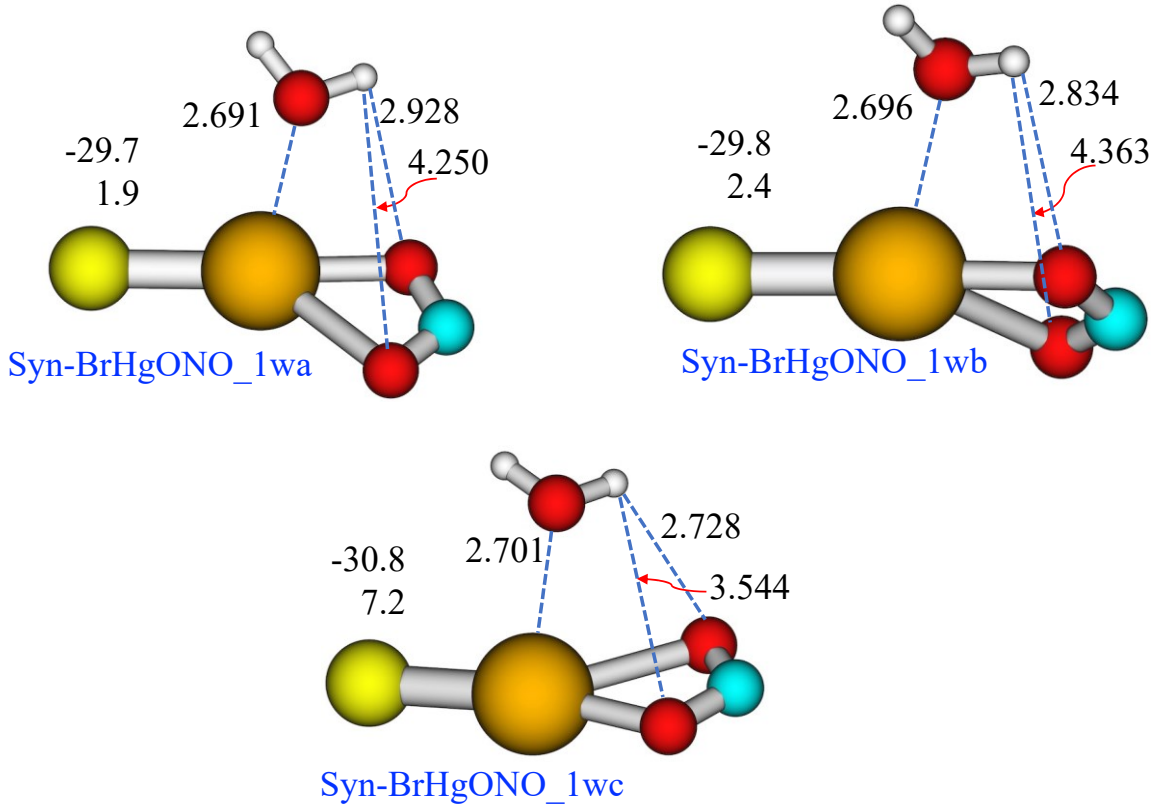

Figure 7. ωB97X-D/aug-cc-pVTZ optimized structures of syn-BrHgONO + H_2O molecular complexes. Atom color-coding as in Fig. 2.

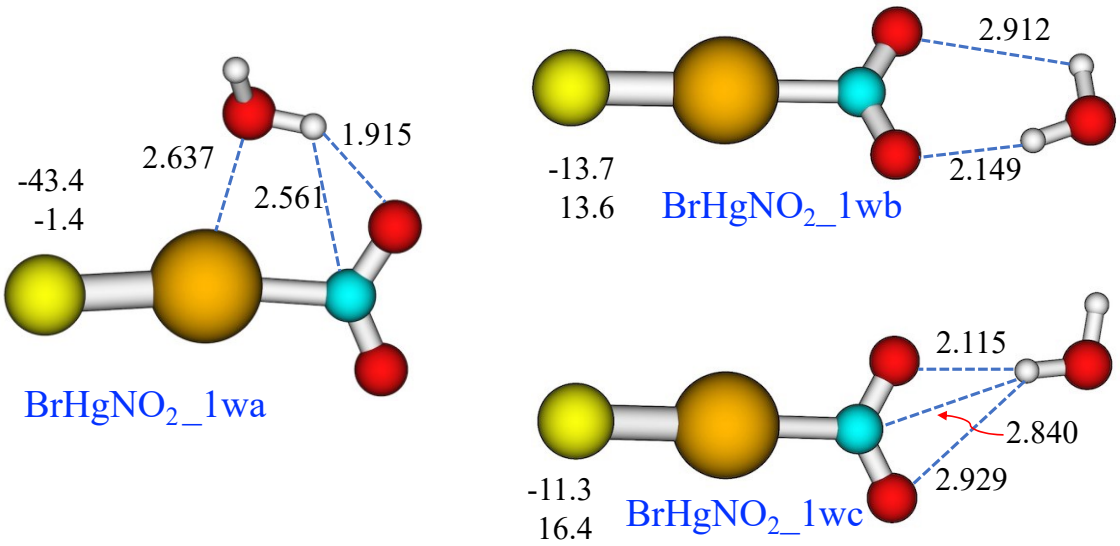

Figure 8. ωB97X-D/aug-cc-pVTZ optimized structures of anti-$BrHgNO_2$ + H_2O molecular complexes. Atom color-coding as in Fig. 2.

Finally, the monohydration of HgOH which does not fall into the preceding groups due to absence of bromine atom, is presented in Figure 9. At the level of electronic energies, in this case, too, the combination ED/PA leads to the most stable mode of bonding.

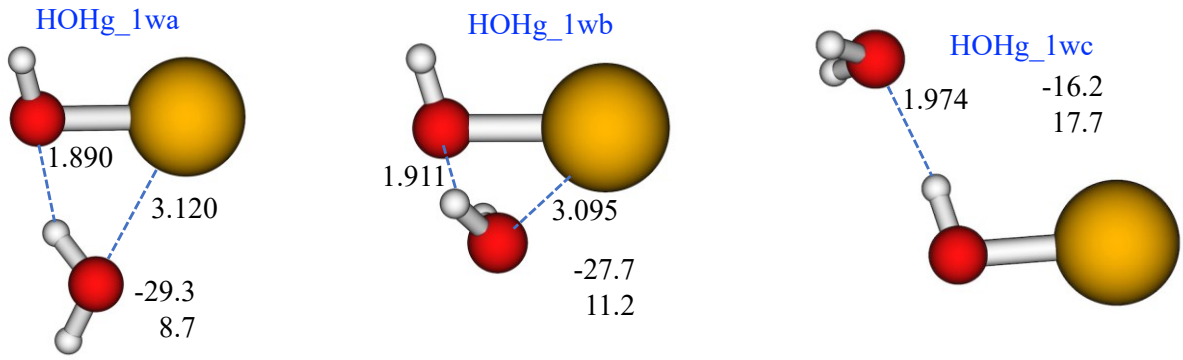

Figure 9. ωB97X-D/aug-cc-pVTZ optimized structures of HOHg + H_2O molecular complexes. Atom color-coding as in Fig. 2.

In Table 1 we present for all the complexes the $\Delta_rH°$ (298 K) and of $\Delta_rG°$ (298 K) values based on the single-point energies calculated at the ωB97X-D/aug-cc-pVTZ//ωB97X-D/aug-cc-pVTZ, DK-CCSD(T)/ANO-RCC-Large//ωB97X-D/aug-cc-pVTZ and DK-CCSD(T)-cf/ANO-RCC-Large//ωB97X-D/aug-cc-pVTZ levels. In Tables 2 and 3 we compare these thermodynamic quantities computed in the range 200-400 K within two approximations: RRHO and QRRHO. Finally, to get the insight into the bonding pattern between water and oxygenated mercury species we present the results of the LMOEDA interaction energy decomposition in Table S17 of the Supporting Information.

IV. DISCUSSION

A. Reactants. Optimized geometric parameters and vibrational frequencies for H_2O at the ωB97X-D/aug-cc-pVTZ level have been already presented in previous studies.[56–58]. The BrHgO geometry was previously computed by Balabanov et *al.*,[59] at CCSD(T)/CBS, and our

geometry compares well with their results. For HOHg, our HgO bond length is longer (by 0.038 Å) than that computed by Dibble et *al*.,[14] at CCSD(T,full)/AwVTZ level. However, the OH distance in those two studies agrees to within 0.002 Å. For the two BrHgONO conformers and BrHgOOH, BrHg distances computed here are 0.014-0.020 Å longer than the CCSD/aug-cc-pVTZ values of Jiao and Dibble.[15] For anti-BrHgONO and BrHgOOH, our HgO distances are 0.017 and 0.013 Å longer, respectively, than the CCSD results, but for *syn*-BrHgONO the analogous HgO distance exceeds the CCSD value by 0.041 Å. Our ωB97X-D harmonic vibrational frequencies agree well with previous work, except for HOHg for which the largest difference between the present work and previous work is 85 cm^{-1}. The moderate differences in geometry parameters and frequencies are not surprising, since the cited theoretical data were obtained either at CCSD or CCSD(T) levels which are clearly superior to DFT model. On the other hand, this computational model is acceptable, bearing in mind the size of hydrated systems and the complexity of their potential energy surface.

B. Monohydration of BrHgO, BrHgOH and BrHgOOH. The LMOEDA decomposition for all three types of monohydrates revealed similar mode of interaction: strong attractive electrostatic and exchange partially compensated by Pauli repulsion (Table S17). Negative polarization and dispersion components contribute to the final total interaction which is stabilizing at the electronic energies level at 0 K. This bonding pattern (combination of electron donor towards mercury with proton acceptor towards oxygen) is similar for all conformers in this group as illustrated in the top row of Figure S10. Addition of all temperature corrections to DK-CCSD(T)-cf/ANO-RCC-Large energies toggles this picture. For instance, two stable structures, BrHgO_1wa and BrHgO_1wb, representing electron donor (water oxygen)/proton acceptor, are indicated as stable at the level of hydration enthalpy. Adding the entropy TΔS term leads to their gradual destabilization at elevated temperatures above 200-240 K and the $\Delta_rG°$ (298 K) is positive for both monohydrates. Note that to hydrate more than 10% of a

molecule at 100% relative humidity and 298 K, $\Delta_rG°(298\ K)$ must be more negative than -3.1 kJ $mole^{-1}$. The importance of the correction for the low-frequency modes is illustrated when comparing Tables 2 and 3, this correction leads to further destabilization of BrHgO_1wa as can be seen in the values of $\Delta_rG°$ in Table 3

Similar LMOEDA-based bonding pattern can be found for BrHgOH and BrHgOOH molecular complexes. Three structures of the monohydrates of BrHgOH and four structures of the monohydrates of BrHgOOH molecular complexes have been identified on the singlet potential energy surface at the ωB97X-D/aug-cc-pVTZ level of theory. Hydrated BrHgOOH structures are similar to BrHgOH ones, in that the water oxygen appears to interact with the Hg atom while the water molecule donates a hydrogen bond to one or both oxygen atoms of BrHgOOH. Here, the decomposition of interaction energy revealed that the ED/PA type of bonding with oxygen on H_2O donating electrons to electrophilic Hg and just one hydrogen bond (hydrogen on H_2O coordinated to OH or OOH groups) is the optimal one giving the most stable 1wa conformers for both the BrHgOH and BrHgOOH (Figures 4, 5 and S10, Table S17).

Addition of the temperature corrections (and also the corrections for low-frequency modes) to DK-CCSD(T)-cf/ANO-RCC-Large energies in these BrHgOH and BrHgOOH molecular complexes has the same effect as in the case of BrHgO. While the hydration enthalpies are still negative, the large TΔS term overturns the energetics and all the complexes in this group become unstable above 220-240 K. The $\Delta_rG°(298\ K)$ becomes positive indicating that even the BrHgOH_1wa and BrHgOOH_1wa with the lowest $\Delta_rH°(298\ K)$ will decompose at ambient temperature after considering the TΔS term.

C. Monohydration of Anti-BrHgONO, Syn-BrHgONO and $BrHgNO_2$. The complexes containing the NO_2-group exhibit several distinctive modes of bonding with water molecule. Dominant one is again the ED mode in which H_2O donates electron pair to mercury, this was

confirmed also by the exploratory MD simulations. In contrast to the previous series, these nitrites and nitro-compounds offer more proton-acceptor sites for water. From the structural point of view, the most stable is the $BrHgNO_2$_1wa which forms quasi-planar 5-membered ring where H_2O donates electron density to Hg via oxygen lone pair and forms the hydrogen bonds towards oxygen and nitrogen in the NO_2 group. The other two conformers ($BrHgNO_2$_1wb and $BrHgNO_2$_1wc) are higher lying local minima that provide only PA interaction suffer from the absence of the direct electron donation towards mercury. The two other BrHgONO conformers (syn and anti) represent competition between ED and PA modes which results in weakening of the total interaction as can be seen also in the components of the interaction energy (Table S17). Figures 6 and 7 further illustrate this point - the distance between hydrogen atom on H_2O and oxygen or nitrogen atoms in NO_2 group in 1wb and/or 1wc conformers are too large to lead to stronger hydrogen bond.

$BrHgNO_2$_1wa binds more strongly to water than any of the other six mercury compounds investigated here (by over 8 kJ mol^{-1}). It possesses (uncorrected for low-frequency modes) $\Delta_rG°$ (298 K) of -1.4 kJ mol^{-1}, which is the only negative value found at 298K for any of the monohydrates we investigated despite having relatively large negative $\Delta_rS°$ (298 K) contribution. Even after including the correction for low-frequency modes this conformer can be thermodynamically stable at temperatures between 200 and 280 K and could survive at tropospheric conditions, especially in polar regions where the increased deposition of mercury oxidized by Br has been observed.

D. Monohydration of HOHg. Three structures have been identified at the ωB97X-D/aug-cc-pVTZ level of theory, and these are shown in Figure 9. Both monohydrates HgOH_1wa and HgOH_1wb are similar to BrHgO_1wb, in that the water oxygen appears to interact with the Hg atom while the water molecule donates a hydrogen bond to HOHg. By contrast, in

HgOH_1wc the water molecule has shifted so that it can accept the proton to form the hydrogen bond via O_w-H-O-Hg linkage with no ED interaction as in HgOH_1wa and HgOH_1wb. This leads to much weaker binding (by 20-26 kJ mol^{-1}) but less negative $\Delta_r S°(298\ K)$ than in conformers a and b. While $\Delta_r G°$ is positive for all three complexes at ambient temperatures, the higher binding energy of HOHg_1wa favors this conformer to coexist in the troposphere at least at low temperatures below 220-210 K (Tables 2 and 3).

E. Atmospheric implications

Table 1. Calculated Standard Reaction Enthalpies and Standard Gibbs Free Reaction Energies at 298 K (in kJ mol^{-1}) at Different Levels of Theory for the Hydration Reactions.

Complex	ωB97X-D/aug-cc-pVTZ		DK-CCSD(T)/ANO-RCC-Large		DK-CCSD(T)-cf/ANO-RCC-Large	
	$\Delta_r H°$(298 K)	$\Delta_r G°$(298 K)	$\Delta_r H°$(298 K)	$\Delta_r G°$(298 K)	$\Delta_r H°$(298 K)	$\Delta_r G°$(298 K)
BrHgO _1wa	–23.0	0.6	–23.7	–0.1	–20.7 (-21.1)	2.9 (6.4)
BrHgO _1wb	–22.9	5.0	–24.8	3.1	–21.8	6.1
BrHgOH _1wa	–26.0	6.7	–28.3	4.3	–25.4 (-25.5)	7.3 (8.2)
BrHgOH_1wb	–19.4	8.1	–17.8	9.6	–14.9	12.6
BrHgOH_1wc	–16.4	12.0	–18.2	10.2	–15.2	13.2
BrHgOOH_1wa	–25.3	5.2	–26.6	3.8	–23.6 (-24.3)	6.8 (12.0)
BrHgOOH_1wb	–31.1	5.4	–31.0	5.5	–28.1	8.4
BrHgOOH_1wc	–29.8	6.5	–30.1	6.2	–27.2	9.1
BrHgOOH_1wd	–25.5	10.3	–26.7	9.1	–23.8	12.0
Anti-BrHgONO_1wa	–28.9	3.4	–30.3	1.9	–27.2 (-27.6)	5.1 (8.0)
Anti-BrHgONO_1wb	–31.9	4.1	–30.4	5.6	–27.3	8.7
Anti-BrHgONO_1wc	–31.9	4.2	–30.3	5.8	–27.2	8.8
Syn-BrHgONO_1wa	–26.2	–0.2	–27.2	–1.2	–24.1 (-25.0)	1.9 (9.3)
Syn-BrHgONO_1wb	–26.2	0.4	–27.3	–0.8	–24.2	2.4
Syn-BrHgONO_1wc	–27.8	4.3	–28.0	4.1	–24.9	7.2
$BrHgNO_2$_1wa	–38.8	–3.1	–40.2	–4.5	–37.0 (-37.3)	–1.4 (2.3)
$BrHgNO_2$_1wb	–10.3	11.3	–11.1	10.4	–7.9	13.6
$BrHgNO_2$_1wc	–7.8	14.3	–8.8	13.2	–5.6	16.4
HOHg_1wa	–24.7	6.9	–25.9	5.6	–22.8 (-23.1)	8.7 (10.4)
HOHg_1wb	–22.7	9.4	–24.0	8.1	–20.9	11.2
HOHg_1wc	–12.0	14.9	–12.1	14.8	–9.2	17.7

Table 2. Calculated Standard Reaction Enthalpies and Standard Gibbs Free Reaction Energies (in kJ mol^{-1}) at different temperatures at the DK-CCSD(T)-cf/ANO-RCC-Large level of theory for the most stable molecular complexes.

Species	BrHgO 1wa		BrHgOH 1wa		BrHgOOH 1wa		Anti-BrHgONO 1wa		Syn-BrHgONO 1wa		$BrHgNO_2$ 1wa		HOHg 1wa	
T (K)	$\Delta_rH°(T)$	$\Delta_rG°(T)$	$\Delta_rH°(T)$	$\Delta_rG°(T)$	$\Delta_rH°(T)$	$\Delta_rG°(T)$	$\Delta_rH°(T)$	$\Delta_rG°(T)$	$\Delta_rH°(T)$	$\Delta_rG°(T)$	$\Delta_rH°(T)$	$\Delta_rG°(T)$	$\Delta_rH°(T)$	$\Delta_rG°(T)$
200	-21.60	-5.06	-26.06	-3.58	-24.53	-3.40	-28.12	-5.72	-25.36	-6.88	-37.54	-13.19	-23.42	-1.81
210	-21.52	-4.23	-26.01	-2.46	-24.46	-2.34	-28.04	-4.60	-25.24	-5.95	-37.51	-11.97	-23.39	-0.73
220	-21.44	-3.41	-25.96	-1.34	-24.39	-1.29	-27.96	-3.48	-25.12	-5.04	-37.48	-10.76	-23.35	0.35
230	-21.36	-2.59	-25.90	-0.22	-24.31	-0.24	-27.87	-2.37	-25.00	-4.13	-37.44	-9.54	-23.30	1.42
240	-21.27	-1.78	-25.84	0.90	-24.22	0.80	-27.78	-1.27	-24.88	-3.22	-37.39	-8.33	-23.25	2.50
250	-21.18	-0.97	-25.77	2.01	-24.13	1.84	-27.68	-0.16	-24.75	-2.32	-37.34	-7.12	-23.19	3.57
260	-21.09	-0.16	-25.69	3.12	-24.03	2.88	-27.58	0.94	-24.62	-1.43	-37.28	-5.91	-23.12	4.64
270	-20.99	0.64	-25.61	4.23	-23.93	3.91	-27.48	2.03	-24.49	-0.54	-37.21	-4.71	-23.05	5.71
280	-20.90	1.44	-25.52	5.33	-23.83	4.94	-27.37	3.12	-24.35	0.34	-37.14	-3.50	-22.98	6.77
290	-20.80	2.24	-25.43	6.43	-23.72	5.97	-27.26	4.21	-24.22	1.22	-37.07	-2.30	-22.90	7.83
298.15	-20.71	2.89	-25.35	7.33	-23.63	6.81	-27.17	5.10	-24.10	1.94	-37.00	-1.35	-22.83	8.70
300	-20.70	3.03	-25.34	7.53	-23.61	6.99	-27.15	5.29	-24.08	2.10	-36.99	-1.11	-22.81	8.89
310	-20.59	3.82	-25.24	8.62	-23.50	8.01	-27.03	6.37	-23.94	2.97	-36.90	0.09	-22.73	9.94
320	-20.49	4.61	-25.14	9.71	-23.38	9.02	-26.91	7.45	-23.80	3.84	-36.81	1.28	-22.63	11.00
330	-20.39	5.39	-25.04	10.80	-23.26	10.04	-26.79	8.52	-23.65	4.70	-36.72	2.47	-22.54	12.05
340	-20.28	6.17	-24.93	11.88	-23.14	11.04	-26.67	9.59	-23.51	5.55	-36.62	3.65	-22.44	13.09
350	-20.17	6.95	-24.82	12.97	-23.02	12.05	-26.54	10.65	-23.36	6.41	-36.52	4.84	-22.34	14.14
360	-20.07	7.72	-24.70	14.04	-22.89	13.05	-26.42	11.71	-23.22	7.26	-36.42	6.02	-22.23	15.18
370	-19.96	8.49	-24.59	15.12	-22.77	14.04	-26.29	12.77	-23.07	8.10	-36.32	7.20	-22.13	16.21
380	-19.85	9.26	-24.47	16.19	-22.64	15.04	-26.16	13.82	-22.92	8.94	-36.21	8.37	-22.02	17.25
390	-19.74	10.02	-24.35	17.26	-22.51	16.03	-26.02	14.87	-22.77	9.78	-36.10	9.54	-21.91	18.28
400	-19.63	10.78	-24.23	18.32	-22.37	17.01	-25.89	15.92	-22.62	10.61	-35.99	10.71	-21.79	19.31

Table 3. Standard Reaction Enthalpies and Standard Gibbs Free Reaction Energies for the most stable molecular complexes (in kJ mol^{-1}) at different temperatures at the DK-CCSD(T)-cf/ANO-RCC-Large level of theory including Truhlar's correction for the low-frequency modes.

Species	BrHgO 1wa		BrHgOH 1wa		BrHgOOH 1wa		Anti-BrHgONO 1wa		Syn-BrHgONO 1wa		$BrHgNO_2$ 1wa		HOHg 1wa	
T (K)	$\Delta_rH°(T)$	$\Delta_rG°(T)$	$\Delta_rH°(T)$	$\Delta_rG°(T)$	$\Delta_rH°(T)$	$\Delta_rG°(T)$	$\Delta_rH°(T)$	$\Delta_rG°(T)$	$\Delta_rH°(T)$	$\Delta_rG°(T)$	$\Delta_rH°(T)$	$\Delta_rG°(T)$	$\Delta_rH°(T)$	$\Delta_rG°(T)$
200	-22.00	-2.83	-26.22	-3.06	-25.13	-0.11	-28.54	-3.93	-26.19	-2.25	-37.84	-10.86	-23.68	-0.78
210	-21.93	-1.87	-26.18	-1.90	-25.07	1.14	-28.46	-2.70	-26.08	-1.06	-37.82	-9.51	-23.65	0.37
220	-21.85	-0.91	-26.13	-0.75	-25.00	2.39	-28.39	-1.48	-25.97	0.13	-37.79	-8.16	-23.62	1.51
230	-21.77	0.04	-26.07	0.41	-24.93	3.63	-28.30	-0.25	-25.85	1.32	-37.75	-6.81	-23.57	2.65
240	-21.69	0.98	-26.01	1.56	-24.85	4.87	-28.21	0.96	-25.73	2.49	-37.71	-5.47	-23.52	3.79
250	-21.60	1.92	-25.94	2.70	-24.76	6.11	-28.12	2.18	-25.61	3.67	-37.66	-4.13	-23.46	4.93
260	-21.51	2.86	-25.86	3.85	-24.67	7.34	-28.02	3.39	-25.48	4.84	-37.60	-2.79	-23.40	6.07
270	-21.41	3.80	-25.78	4.99	-24.57	8.57	-27.92	4.59	-25.35	6.00	-37.53	-1.45	-23.33	7.20
280	-21.32	4.73	-25.70	6.13	-24.47	9.80	-27.82	5.80	-25.22	7.16	-37.46	-0.12	-23.26	8.33
290	-21.22	5.66	-25.61	7.26	-24.36	11.02	-27.71	6.99	-25.09	8.31	-37.39	1.22	-23.18	9.45
298.15	-21.14	6.41	-25.53	8.18	-24.28	12.01	-27.62	7.97	-24.98	9.25	-37.33	2.30	-23.11	10.37
300	-21.12	6.58	-25.51	8.39	-24.26	12.24	-27.60	8.19	-24.95	9.46	-37.31	2.55	-23.10	10.58
310	-21.02	7.51	-25.42	9.52	-24.14	13.45	-27.48	9.38	-24.82	10.61	-37.23	3.87	-23.01	11.70
320	-20.92	8.42	-25.32	10.65	-24.03	14.66	-27.36	10.57	-24.68	11.75	-37.14	5.20	-22.92	12.82
330	-20.82	9.34	-25.21	11.77	-23.91	15.87	-27.24	11.75	-24.54	12.88	-37.05	6.52	-22.83	13.93
340	-20.71	10.25	-25.10	12.89	-23.80	17.07	-27.12	12.93	-24.40	14.02	-36.95	7.84	-22.73	15.05
350	-20.61	11.16	-24.99	14.00	-23.67	18.27	-27.00	14.11	-24.25	15.14	-36.86	9.16	-22.63	16.15
360	-20.50	12.07	-24.88	15.12	-23.55	19.47	-26.87	15.28	-24.11	16.27	-36.75	10.47	-22.53	17.26
370	-20.39	12.97	-24.77	16.23	-23.42	20.66	-26.75	16.45	-23.96	17.39	-36.65	11.78	-22.42	18.36
380	-20.28	13.87	-24.65	17.33	-23.30	21.85	-26.62	17.61	-23.82	18.50	-36.54	13.09	-22.31	19.47
390	-20.17	14.77	-24.53	18.44	-23.17	23.04	-26.48	18.78	-23.67	19.62	-36.43	14.39	-22.20	20.56
400	-20.06	15.67	-24.41	19.54	-23.04	24.22	-26.35	19.94	-23.52	20.72	-36.32	15.69	-22.08	21.66

IV. CONCLUSIONS

Our combined survey (ESP maps, molecular dynamics and systematic scan of the molecular exterior) unambiguously revealed that for the first water molecule are Hg, HgO and $HgNO_2$ moieties the favorable hydrophilic sites, while bromine is in all cases hydrophobic. 22 molecular complexes have been identified on the ground state potential energy surface. The thermodynamic properties of the total hydration reactions of mercury species with one water molecule in the temperature range 200-400 K (standard reaction enthalpy $\Delta_rH°(298\ K)$ and standard Gibbs free energy $\Delta_rG°(298\ K)$) were calculated at the ωB97X-D/aug-cc-pVTZ, DK-CCSD(T)/ANO-RCC-Large, and DK-CCSD(T)-cf/ANO-RCC-Large levels on ωB97X-D/aug-cc-pVTZ optimized geometries. DK-CCSD(T)-cf binding energies exceed ωB97X-D values by 0.6 to 4.7 kJ mol^{-1}, with an average value of 2.4 ± 1.1 kJ mol^{-1}. The continued fraction approximation increases CCSD(T) binding energies by about 3 kJ mol^{-1}. Our results for $\Delta_rH°$ show that all monohydration processes of mercury species are exothermic at 298 K in standard conditions whatever the level of theory, these moderate enthalpies of hydration in the range of -20 to -37 kJ mol^{-1} indicate relatively weak intermolecular interactions between water and bromo-oxygenated mercury compounds. Entropy term plays key role in determining the conditions of thermodynamic equilibrium in terms of $\Delta_rG°$ - inclusion of the entropy term $T\Delta S$ overturned negative enthalpies and monohydration is characterized by $\Delta_rG°(298\ K) > 0$ for all conformers of all compounds studied here. The only exception is the stable though weakly bound conformer $BrHgNO_2$ ($BrHgNO_2$_1wa ($\Delta_rG°(298\ K)$ = -1.4 kJ mol^{-1})). Although the hydration reactions of Syn-BrHgONO and BrHgO possess negative values of $\Delta_rG°$ at temperatures below 260-270 K, these hydration reactions cannot be spontaneous under atmospheric conditions due to the low equilibrium vapor pressure of water ice. Our results indicate that, at 298 K and 100% relative humidity, only 5% of $BrHgNO_2$ could exist as the

hydrate. The next nearest value of $\Delta_r G°(298\ K)$ (+ 0.7 kJ mol^{-1}) occurs for HOHg_1wb, which should constitute 2% of all HOHg at 298 K and 100% relative humidity. These results suggest that at the temperatures above 200K the monohydration of HOHg, $BrHgNO_2$, BrHgONO, BrHgOH, BrHgOOH, and BrHgO is not important in the atmosphere and that $BrHgNO_2$ is most likely to exist in the hydrated forms under tropospheric conditions. The results obtained here can be used to validate efficient force fields or lower levels of quantum chemistry for use in studying the chemistry of these species in aqueous solution or on wetted surfaces.

AUTHOR INFORMATION

Corresponding Author: ivan.cernusak@uniba.sk

ORCID

Sonia Taamalli: 0000-0002-6200-7115

Michal Pitoňák: 0000-0002-0601-9488

Florent Louis 0000-0002-9533-557X

Theodore S. Dibble 0000-0002-0023-8233

Ivan Černušák 0000-0002-6597-3095

Notes

The authors declare no competing financial interest.

Supporting Information Available: Optimized geometry parameters (Table S1) and vibrational frequencies (Table S2) for BrHgO, BrHgOH, BrHgOOH, BrHgONO with two conformers (syn and anti), $BrHgNO_2$ and HOHg. Optimized Cartesian coordinates and vibrational frequencies (Tables S3 – S16) for the mono-hydrated structures of BrHgO, BrHgOH, BrHgOOH, BrHgONO with two conformers (syn and anti), $BrHgNO_2$ and HOHg. LMOEDA components of the interaction energy for the monohydrated structures are in Table

S17. Model IR spectra of all the structures (non-hydrated and mono-hydrated) are collected in Figures S1 – S9. Color-coded electrostatic potential maps of the most stable mono-hydrated structures projected onto electron density are summarized in Figure S10.

ACKNOWLEDGMENTS

The authors thank Ms. Aurélie Lobbestael for providing preliminary work on the studied molecular systems. Computer time for part of the theoretical calculations was kindly provided by the Centre de Ressources Informatiques (CRI) of the University of Lille and the Centre Régional Informatique et d'Applications Numériques de Normandie (CRIANN). We appreciated the support from the French ANR agency under Contract No. ANR-11-LABX-0005 “Chemical and Physical Properties of the Atmosphere” (CaPPA). This work was granted access to the HPC resources of IDRIS under the allocation 2020-101578 made by GENCI. This work was supported in part by the Slovak Grant Agency VEGA (grant 1/0777/19) and by the high-performance computing facility of the Centre for Information Technology (https://uniba.sk/en/HPC-Clara) at Comenius University. Molecular dynamics calculations were performed in the Centre of Operations of the Slovak Academy of Sciences using the supercomputing infrastructure acquired in projects ITMS 26230120002 and 26210120002 supported by the Research & Development Operational Programme funded by the ERDF. TSD thanks the US National Science Foundation for their support under award 2004100.

References

(1) Driscoll, C. T.; Mason, R. P.; Chan, H. M.; Jacob, D. J.; Pirrone, N. Mercury as a Global Pollutant: Sources, Pathways, and Effects. *Environ. Sci. Technol.* **2013**, *47* (10), 4967–4983.

(2) Lin, C.-J.; Pongprueksa, P.; Lindberg, S. E.; Pehkonen, S. O.; Byun, D.; Jang, C. Scientific Uncertainties in Atmospheric Mercury Models I: Model Science Evaluation. *Atmos. Environ.* **2006**, *40* (16), 2911–2928.

(3) Horowitz, H. M.; Jacob, D. J.; Zhang, Y.; Dibble, T. S.; Slemr, F.; Amos, H. M.; Schmidt, J. A.; Corbitt, E. S.; Marais, E. A.; Sunderland, E. M. A New Mechanism for Atmospheric Mercury

Redox Chemistry: Implications for the Global Mercury Budget. *Atmospheric Chem. Phys.* **2017**, *17* (10), 6353–6371.

(4) Saiz-Lopez, A.; Travnikov, O.; Sonke, J. E.; Thackray, C. P.; Jacob, D. J.; Carmona-García, J.; Francés-Monerris, A.; Roca-Sanjuán, D.; Acuña, A. U.; Dávalos, J. Z.; et al. Photochemistry of Oxidized Hg(I) and Hg(II) Species Suggests Missing Mercury Oxidation in the Troposphere. *Proc. Natl. Acad. Sci.* **2020**, *117* (49), 30949–30956.

(5) Thomsen, D. L.; Kurtén, T.; Jørgensen, S.; Wallington, T. J.; Baggesen, S. B.; Aalling, C.; Kjaergaard, H. G. On the Possible Catalysis by Single Water Molecules of Gas-Phase Hydrogen Abstraction Reactions by OH Radicals. *Phys. Chem. Chem. Phys.* **2012**, *14* (37), 12992–12999.

(6) Kjaergaard, H. G.; Robinson, T. W.; Howard, D. L.; Daniel, J. S.; Headrick, J. E.; Vaida, V. Complexes of Importance to the Absorption of Solar Radiation †. *J. Phys. Chem. A* **2003**, *107* (49), 10680–10686.

(7) Buszek, R.; Francisco, J.; Anglada, J. Water Effects on Atmospheric Reactions. *Int. Rev. Phys. Chem. - INT REV PHYS CHEM* **2011**, *30*, 335–369.

(8) Zhu, R.; Lin, M. C. Ab Initio Study of the Catalytic Effect of H2O on the Self-Reaction of HO2. *Chem. Phys. Lett.* **2002**, *354* (3), 217–226.

(9) Chao, W.; Yin, C.; Takahashi, K.; Lin, J. J.-M. Hydrogen-Bonding Mediated Reactions of Criegee Intermediates in the Gas Phase: Competition between Bimolecular and Termolecular Reactions and the Catalytic Role of Water. *J. Phys. Chem. A* **2019**, *123* (39), 8336–8348.

(10) Kürten, A.; Li, C.; Bianchi, F.; Curtius, J.; Dias, A.; Donahue, N. M.; Duplissy, J.; Flagan, R. C.; Hakala, J.; Jokinen, T.; et al.New Particle Formation in the Sulfuric Acid–Dimethylamine–Water System: Reevaluation of CLOUD Chamber Measurements and Comparison to an Aerosol Nucleation and Growth Model. *Atmospheric Chem. Phys.* **2018**, *18* (2), 845–863.

(11) Lehtipalo, K.; Rondo, L.; Kontkanen, J.; Schobesberger, S.; Jokinen, T.; Sarnela, N.; Kürten, A.; Ehrhart, S.; Franchin, A.; Nieminen, T.; et al.The Effect of Acid–Base Clustering and Ions on the Growth of Atmospheric Nano-Particles. *Nat. Commun.* **2016**, *7* (1), 11594.

(12) Dibble, T. S.; Zelie, M. J.; Mao, H. Thermodynamics of Reactions of ClHg and BrHg Radicals with Atmospherically Abundant Free Radicals. *Atmospheric Chem. Phys.* **2012**, *12* (21), 10271–10279.

(13) Moore, C. W.; Obrist, D.; Luria, M. Atmospheric Mercury Depletion Events at the Dead Sea: Spatial and Temporal Aspects. *Atmos. Environ.* **2013**, *69*, 231–239.

(14) Dibble, T. S.; Tetu, H. L.; Jiao, Y.; Thackray, C. P.; Jacob, D. J. Modeling the OH-Initiated Oxidation of Mercury in the Global Atmosphere without Violating Physical Laws. *J. Phys. Chem. A* **2020**, *124* (2), 444–453.

(15) Jiao, Y.; Dibble, T. S. Quality Structures, Vibrational Frequencies, and Thermochemistry of the Products of Reaction of BrHg $^{\bullet}$ with NO_2 , HO_2 , ClO, BrO, and IO. *J. Phys. Chem. A* **2015**, *119* (42), 10502–10510.

(16) Lam, K. T.; Wilhelmsen, C. J.; Schwid, A. C.; Jiao, Y.; Dibble, T. S. Computational Study on the Photolysis of BrHgONO and the Reactions of $BrHgO^{\bullet}$ with CH_4 , C_2H_6 , NO, and NO_2 : Implications for Formation of Hg(II) Compounds in the Atmosphere. *J. Phys. Chem. A* **2019**, *123* (8), 1637–1647.

(17) Francés-Monerris, A.; Carmona-García, J.; Acuña, A. U.; Dávalos, J. Z.; Cuevas, C. A.; Kinnison, D. E.; Francisco, J. S.; Saiz-Lopez, A.; Roca-Sanjuán, D. Photodissociation Mechanisms of Major Mercury(II) Species in the Atmospheric Chemical Cycle of Mercury. *Angew. Chem. Int. Ed.* **2020**, *59* (19), 7605–7610.

(18) Tacey, S. A.; Xu, L.; Mavrikakis, M.; Schauer, J. J. Heterogeneous Reduction Pathways for Hg(II) Species on Dry Aerosols: A First-Principles Computational Study. *J. Phys. Chem. A* **2016**, *120* (13), 2106–2113.

(19) Rubasinghege, G.; Grassian, V. H. Role(s) of Adsorbed Water in the Surface Chemistry of Environmental Interfaces. *Chem. Commun.* **2013**, *49* (30), 3071–3094.
(20) Sumner, A. L.; Menke, E. J.; Dubowski, Y.; Newberg, J. T.; Penner, R. M.; Hemminger, J. C.; Wingen, L. M.; Brauers, T.; Finlayson-Pitts, B. J. The Nature of Water on Surfaces of Laboratory Systems and Implications for Heterogeneous Chemistry in the Troposphere. *Phys. Chem. Chem. Phys.* **2004**, *6* (3), 604–613.
(21) Fujita, S.; Horii, H.; Mori, T.; Taniguchi, S. Pulse Radiolysis of Mercuric Oxide in Neutral Aqueous Solutions. *J. Phys. Chem.* **1975**, *79* (10), 960–964.
(22) Clarke, J. H. R.; Woodward, L. A. Raman Spectra of Monohalide Complexes of Mercury (II) in Aqueous Solution. *Trans. Faraday Soc.* **1965**, *61* (0), 207–211.
(23) Tossell, J. A. Theoretical Studies on the Formation of Mercury Complexes in Solution and the Dissolution and Reactions of Cinnabar. *Am. Mineral.* **1999**, *84* (5–6), 877–883.
(24) Tossell, J. A. Calculation of the Structures, Stabilities, and Properties of Mercury Sulfide Species InAqueous Solution. *J. Phys. Chem. A*. 2001, pp 935–941.
(25) Afaneh, A. T.; Schreckenbach, G.; Wang, F. Density Functional Study of Substituted (–SH, –S, –OH, –Cl) Hydrated Ions of Hg^{2+}. *Theor. Chem. Acc.* **2012**, *131* (4), 1174.
(26) Shepler, B. C.; Wright, A. D.; Balabanov, N. B.; Peterson, K. A. Aqueous Microsolvation of Mercury Halide Species. *J. Phys. Chem. A* **2007**, *111* (44), 11342–11349.
(27) Soldán, P.; Lee, E. P. F.; Wright, T. G. Microsolvation of Hg and Hg^{2+}: Energetics of $Hg{\cdot}H_2O$, $Hg^{2+}{\cdot}H_2O$ and $HgOH^+$. *J. Phys. Chem. A* **2002**, *106* (37), 8619–8626.
(28) Chai, J.-D.; Head-Gordon, M. Long-Range Corrected Hybrid Density Functionals with Damped Atom–Atom Dispersion Corrections. *Phys. Chem. Chem. Phys.* **2008**, *10* (44), 6615–6620.
(29) Gaussian 16, Revision C.01, Frisch, M. J.; Trucks, G. W.; Schlegel, H. B.; Scuseria, G. E.; Robb, M. A.; Cheeseman, J. R.; Scalmani, G.; Barone, V.; Petersson, G. A.; Nakatsuji, H.; et al. Gaussian, Inc., Wallingford CT, **2016**.
(30) Minenkov, Y.; Singstad, Å.; Occhipinti, G.; Jensen, V. R. The Accuracy of DFT-Optimized Geometries of Functional Transition Metal Compounds: A Validation Study of Catalysts for Olefin Metathesis and Other Reactions in the Homogeneous Phase. *Dalton Trans.* **2012**, *41* (18), 5526.
(31) Mardirossian, N.; Head-Gordon, M. Thirty Years of Density Functional Theory in Computational Chemistry: An Overview and Extensive Assessment of 200 Density Functionals. *Mol. Phys.* **2017**, *115* (19), 2315–2372.
(32) Peterson, K. A.; Figgen, D.; Goll, E.; Stoll, H.; Dolg, M. Systematically Convergent Basis Sets with Relativistic Pseudopotentials. II. Small-Core Pseudopotentials and Correlation Consistent Basis Sets for the Post-d Group 16–18 Elements. *J. Chem. Phys.* **2003**, *119* (21), 11113–11123.
(33) Dunning, T. H. Gaussian Basis Sets for Use in Correlated Molecular Calculations. I. The Atoms Boron through Neon and Hydrogen. *J. Chem. Phys.* **1989**, *90* (2), 1007–1023.
(34) Figgen, D.; Rauhut, G.; Dolg, M.; Stoll, H. Energy-Consistent Pseudopotentials for Group 11 and 12 Atoms: Adjustment to Multi-Configuration Dirac–Hartree–Fock Data. *Chem. Phys.* **2005**, *311* (1–2), 227–244.
(35) Peterson, K. A.; Shepler, B. C.; Figgen, D.; Stoll, H. On the Spectroscopic and Thermochemical Properties of ClO, BrO, IO, and Their Anions. *J. Phys. Chem. A* **2006**, *110* (51), 13877–13883.
(36) Ryjáček, F.; Engkvist, O.; Vacek, J.; Kratochvíl, M.; Hobza, P. Hoogsteen and Stacked Structures of the 9-Methyladenine···1-Methylthymine Pair Are Populated Equally at Experimental Conditions: Ab Initio and Molecular Dynamics Study. *J. Phys. Chem. A* **2001**, *105* (7), 1197–1202.
(37) Perdew, J. P.; Burke, K.; Ernzerhof, M. Generalized Gradient Approximation Made Simple. *Phys. Rev. Lett.* **1996**, *77* (18), 3865–3868.

(38) Perdew, J. P.; Ruzsinszky, A.; Csonka, G. I.; Vydrov, O. A.; Scuseria, G. E.; Constantin, L. A.; Zhou, X.; Burke, K. Restoring the Density-Gradient Expansion for Exchange in Solids and Surfaces. *Phys. Rev. Lett.* **2008**, *100* (13), 136406.
(39) Zhang, Y.; Yang, W. Comment on ``Generalized Gradient Approximation Made Simple''. *Phys. Rev. Lett.* **1998**, *80* (4), 890–890.
(40) Becke, A. D. Density-functional Thermochemistry. III. The Role of Exact Exchange. *J. Chem. Phys.* **1993**, *98* (7), 5648–5652.
(41) VandeVondele, J.; Hutter, J. Gaussian Basis Sets for Accurate Calculations on Molecular Systems in Gas and Condensed Phases. *J. Chem. Phys.* **2007**, *127* (11), 114105.
(42) Kühne, T. D.; Iannuzzi, M.; Del Ben, M.; Rybkin, V. V.; Seewald, P.; Stein, F.; Laino, T.; Khaliullin, R. Z.; Schütt, O.; Schiffmann, F.; et al. CP2K: An Electronic Structure and Molecular Dynamics Software Package - Quickstep: Efficient and Accurate Electronic Structure Calculations. *J. Chem. Phys.* **2020**, *152* (19), 194103.
(43) T. H. Dunning Jr. and P. J. Hay, In: H. F. Schaefer III, Ed., *Methods of Electronic Structure Theory*, *Vol. 2*, Plenum Press, **1977**.
(44) Hay, P. J.; Wadt, W. R. Ab Initio Effective Core Potentials for Molecular Calculations. Potentials for the Transition Metal Atoms Sc to Hg. *J. Chem. Phys.* **1985**, *82* (1), 270–283.
(45) Wadt, W. R.; Hay, P. J. Ab Initio Effective Core Potentials for Molecular Calculations. Potentials for Main Group Elements Na to Bi. *J. Chem. Phys.* **1985**, *82* (1), 284–298.
(46) Hay, P. J.; Wadt, W. R. Ab Initio Effective Core Potentials for Molecular Calculations. Potentials for K to Au Including the Outermost Core Orbitals. *J. Chem. Phys.* **1985**, *82* (1), 299–310.
(47) MacQueen, J. Some Methods for Classification and Analysis of Multivariate Observations. *Proc. Fifth Berkeley Symp. Math. Stat. Probab. Vol. 1 Stat.* **1967**, 281–297.
(48) Lucien M., L. C.; Neyman, J. Proceedings of the Fifth Berkeley Symposium on Mathematical Statistics and Probability, Volume 2: Contributions to Probability Theory, Part 1. *Berkeley Symp. on Math. Statist. and Prob.* 2A 1967, p 447pp.
(49) Aquilante, F.; Vico, L. D.; Ferré, N.; Ghigo, G.; Malmqvist, P.-åke; Neogrády, P.; Pedersen, T. B.; Pitoňák, M.; Reiher, M.; Roos, B. O.; et al. MOLCAS 7: The Next Generation. *J. Comput. Chem.* **2010**, *31* (1), 224–247.
(50) Bjo1rnO., R.; Roland, L.; Per-A°ke, M.; Valera, V.; Per-Olof, W. Main Group Atoms and Dimers Studied with a New Relativistic ANO Basis Set. *J. Phys. Chem. A* **2004**, 108*, 15, 2851–2858*
(51) Goodson, D. Z. Extrapolating the Coupled-Cluster Sequence toward the Full Configuration-Interaction Limit. *J. Chem. Phys.* **2002**, *116* (16), 6948–6956.
(52) Ribeiro, R. F.; Marenich, A. V.; Cramer, C. J.; Truhlar, D. G. Use of Solution-Phase Vibrational Frequencies in Continuum Models for the Free Energy of Solvation. *J. Phys. Chem. B* **2011**, *115* (49), 14556–14562.
(53) Lu, T.; Chen, Q. Shermo: A General Code for Calculating Molecular Thermochemistry Properties. *Comput. Theor. Chem.* **2021**, *1200*, 113249.
(54) Su, P.; Li, H. Energy Decomposition Analysis of Covalent Bonds and Intermolecular Interactions. *J. Chem. Phys.* **2009**, *131* (1), 014102.
(55) Stevens, W. J.; Krauss, M.; Basch, H.; Jasien, P. G. Relativistic Compact Effective Potentials and Efficient, Shared-Exponent Basis Sets for the Third-, Fourth-, and Fifth-Row Atoms. *Can. J. Chem.* **1992**, *70* (2), 612–630.
(56) Villard, A.; Khanniche, S.; Fortin, C.; Cantrel, L.; Černušák, I.; Louis, F. A Theoretical Study of the Microhydration Processes of Iodine Nitrogen Oxides. *Int. J. Quantum Chem.* **2019**, *119* (3), e25792.

(57) Khiri, D.; Vandeputte, R.; Taamalli, S.; Cantrel, L.; Louis, F. Microhydration of Caesium Metaborate Structural and Thermochemical Properties of $CsBO_2$ + n H_2O (n = 1–4) Aggregates. *J. Mol. Model.* **2019**, *25* (7), 207.
(58) Taamalli, S.; Khiri, D.; Suliman, S.; Khanniche, S.; Černušák, I.; Cantrel, L.; Ribaucour, M.; Louis, F. Unraveling the Tropospheric Microhydration Processes of Iodous Acid HOIO. *ACS Earth Space Chem.* **2020**, *4* (1), 92–100.
(59) Balabanov, N. B.; Shepler, B. C.; Peterson, K. A. Accurate Global Potential Energy Surface and Reaction Dynamics for the Ground State of $HgBr_2$. *J. Phys. Chem. A* **2005**, *109* (39), 8765–8773.